

Colossal nonreciprocal Hall effect and the breakdown of Ohm's law due to a room temperature nonlinear Hall effect

Lujin Min^{1,2}, Yang Zhang³, Zhijian Xie⁴, Leixin Miao², Yugo Onishi³, Nasim Alem², Liang Fu^{3*}, Zhiqiang Mao^{1,2*}

¹Department of Physics, Pennsylvania State University; University Park, PA, USA

²Department of Materials Science and Engineering, Pennsylvania State University; University Park, PA, USA

³Department of Physics, Massachusetts Institute of Technology, Cambridge, MA, USA

⁴Department of Electrical and Computer Engineering, North Carolina Agriculture & Technical State University, Greensboro, NC, USA

Abstract

Nonreciprocal charge transport in quantum materials has attracted enormous interest since it offers an avenue to investigate quantum symmetry related physics and holds many prospective applications such as rectification and photodetection over a wide range of frequencies.¹ The nonreciprocal transport reported to date occurs along the longitudinal direction with the nonreciprocal resistance limited to a few percent of the ohmic resistance.² Here we report a transverse nonreciprocal transport phenomenon with divergent nonreciprocity – colossal nonreciprocal Hall effect. This is revealed in direct current (DC) transport measurements on microscale crystals of the Weyl semimetal NbP at zero magnetic field. When a DC (I_a) is applied along its a -axis, it generates a voltage along the c -axis (V_c) near room temperature, with V_c quadratically scaling with I_a . The transverse resistance, which shows a sign reversal upon switching the current direction, results from a colossal intrinsic nonlinear Hall effect (NLHE) rooted in the band topology and quantum symmetry. Such a NLHE yields an exceptionally large Hall angle θ_H , e.g. $\theta_H = 39^\circ$ at $I_a = 1$ mA at 330K, far exceeding the record value ($\sim 12^\circ$) of the anomalous Hall angle at room temperature in magnetic conductors.³ Furthermore, we find the large Hall field also results in an unprecedented bulk electrical field effect, which increases the longitudinal conductivity, thus causing the breakdown of Ohm's law. These results not only demonstrate the concept of nonreciprocal Hall effect for the first time but also pave the way for developing NLHE-based quantum sensors for transformative advancement in communication technology and energy harvesting.

* Corresponding authors. Email: liangfu@mit.edu (L.F.); zim1@psu.edu (Z.Q.M.)

Ohm's law is the most fundamental law governing electrical transport in materials and electronic circuits. It states that under a constant condition, the current flowing through a conductor is linearly proportional to the voltage across the two ends of the conductor when heating and junction effects are excluded. However, in non-centrosymmetric polar materials, there is a mechanism that can cause an experimentally observable deviation from Ohm's law under magnetic fields, i.e. the nonreciprocal transport.^{2,4} When the applied current \mathbf{I} and magnetic field \mathbf{B} are perpendicular to each other and orthogonal to the polar axis \mathbf{P} of a given polar material, as illustrated in Fig. 1a, the current-voltage (I - V) characteristic measured with a direct current (DC) can be described by $V = R_0 I + \gamma R_0 B I^2$ where γ is a coefficient (Fig. 1b).² The corresponding resistance $R(I) \equiv \frac{V}{I} = R_0 + \gamma R_0 B I$ depends on the direction of the current, resulting in nonreciprocal transport. The degree of nonreciprocity is characterized by the ratio of the nonreciprocal resistance to the ohmic resistance: $\eta = \frac{R(I) - R(-I)}{R(I) + R(-I)}$. The value of η is usually very small such that the violation of Ohm's law is hardly observable in DC transport measurements.⁵ The nonreciprocal transport phenomena reported so far are instead probed by alternating current (AC) transport measurements.⁵⁻¹⁰

Recently, a second-order transverse transport phenomenon induced by Berry curvature effect, i.e. the so-called nonlinear Hall effect (NLHE), was proposed for noncentrosymmetric but time-reversal-invariant quantum materials.¹¹ Considering a material with a polar axis \mathbf{P} , when a DC I_x is applied perpendicular to \mathbf{P} , a transverse voltage V_y proportional to the square of the current develops along \mathbf{P} , as shown in Fig. 1c. The quadratic dependence $V_y \propto I_x^2$ (Fig. 1d) is a fundamental violation of Ohm's law. Importantly, upon reversing the direction of the applied current I_x the transverse voltage is symmetric to I_x , so that the transverse resistance $R_{yx} \equiv \frac{V_y}{I_x} \propto I_x$ changes sign, thus leading to a divergent transverse nonreciprocity as defined by $\eta_H \equiv \frac{R_{yx}(I_x) - R_{yx}(-I_x)}{R_{yx}(I_x) + R_{yx}(-I_x)} \rightarrow \infty$. Such nonreciprocal transverse DC transport can be termed as a nonreciprocal Hall effect. While the NLHE has been observed in several material systems through AC transport measurements¹²⁻²⁰, there have been no reports on DC I - V characteristics that demonstrate the transverse nonreciprocity. Furthermore, the reported NLHEs are primarily low-temperature phenomena. Room-temperature NLHEs were seen only in exfoliated TaIrTe₄ flakes¹⁴ and BaMnSb₂ bulk single crystals²⁰. Nevertheless, even at the maximum applied current, the NLHE-induced transverse voltage in these materials is still orders of magnitude smaller than the longitudinal voltage at linear response, which prevents observation of the nonreciprocal Hall effect and limits the potential for NLHE-based applications.

In this work, we report a room-temperature colossal NLHE observed in the Weyl semimetal NbP and demonstrate its resulting nonreciprocal Hall effect through DC transport measurements on micrometer-scale Hall devices. Our results show that the NLHE of NbP leads to a surprisingly large, current-dependent Hall angle θ_H , e.g. $\theta_H = 39^\circ$ at $I_a = 1$ mA and 330 K, which far exceeds the record value ($\sim 12^\circ$) of the anomalous Hall angle in magnetic conductors at room temperature. Thanks to this colossal nonlinear Hall response, the sign reversal of the transverse resistance R_{yx} as well as divergent η_H are also clearly observed. Furthermore, we have also discovered a *bulk electric field effect* induced by the large Hall field, which leads to sublinear I_x - V_x characteristics,

thus violating Ohm's law. Additionally, the colossal NLHE of NbP at room temperature highlights the tremendous potential of using nonlinear Hall devices as quantum sensors for terahertz (THz) detection and energy harvesting.

Our study on NbP's NLHE was inspired by Zhang and Fu's recent prediction¹ that the gapped nodal rings near the Fermi energy of this material generate a large net Berry curvature dipole (BCD), which is expected to drive a strong nonlinear Hall voltage response along its polar axis (i.e. c -axis) as the current is applied to the plane perpendicular to the c -axis, as illustrated in Fig. 2a. Therefore, this material may serve as a platform for the demonstration of the nonreciprocal Hall effect. Under this motivation, we fabricated micrometer scale Hall devices of NbP single crystals through focused ion beam (FIB) machining (see Methods and Supplementary Note 1). The use of small dimensions of the devices aims to access a high current density, which is critical to the observation of the predicted NLHE (Supplementary Note 1). Fig. 1e shows an image of a representative cross-shape Hall device (S1) with two pairs of arms that are approximately parallel to the crystallographic a and c -axis, respectively. The Pt contacts and wires attached on the device were deposited as described in Methods. The contacts of the device in Fig. 1e are labeled for the Hall voltage measurements with the current applied along the a -axis.

Using such a micro-scale Hall device, we successfully observed a colossal nonreciprocal Hall effect near room temperature when the current was applied along the a -axis. In Fig 1f, we present the DC I - V characteristics measured at various temperatures on device S1. When the temperature is ≤ 200 K, the I - V curves exhibit linear dependences, consistent with the expected Ohm's law behavior. In stark contrast, as the temperature is increased above 200K, the I - V curves start to significantly deviate from linear behavior and such a deviation reaches a maximum at temperatures close to 350K where the I - V curves are parabolic-like. Such a parabolic-like I - V curve becomes much more remarkable in a large current range (see Fig. 1h). By symmetrizing and anti-symmetrizing the measured data, the measured transverse voltage V_c can be decomposed into a quadratic voltage component $V_c^{QD} (\propto I_a^2)$ (see Fig. 1i) and a linear voltage component $V^L (\propto I_a)$ (see Fig. 1j which displays the V^L component only at 350K as an example). As to be discussed below, V_c^{QD} corresponds to the second-order Hall voltage response caused by the NLHE, while V^L is attributable to the unavoidable electrical contacts' misalignment. The nonreciprocal Hall response observed here is so strong that V^{QD} is even larger than V^L , e.g., $V^{QD}/V^L = 1.58$ at 350K and 50 μ A. Moreover, the I - V characteristics near 350 K clearly demonstrate the signal reversal of the transverse Hall resistance between negative and positive currents. From the raw I - V curve at 350 K, the nonreciprocity coefficient η_H is estimated to be 160% for $I_a = 50$ μ A and 1800% for 500 μ A (Fig. 1h), which is several orders of magnitude larger than the previously reported nonreciprocity η for longitudinal nonreciprocal transport (see Supplementary Table 2). In the absence of contacts' misalignment, the transverse voltage is quadratic in the applied current ($V_c^{QD} \propto I_a^2$) (Fig. 1h), so that η_H is infinitely large. All these features agree well with the expected nonreciprocal Hall effect.

Our detailed experimental studies further prove that such a nonreciprocal Hall effect is caused by an intrinsic NLHE, as discussed in Supplementary Note 2. According to the theory by Zhang and Fu¹, the NLHE of NbP is dependent on the current direction: its nonlinear Hall response is maximal

when the current is applied to the plane perpendicular to the c -axis but absent as the current is applied along the c -axis (see Supplementary Note 2). To verify this, we performed DC transport measurements with $I//c$. In contrast to the measurements with $I//a$ (Fig. 1f), the I - V curves measured with $I//c$ remained almost linear in the whole temperature range, as shown in Fig. 1g. Only a very small deviation from linearity was observed near 350K. We also extracted the V^{QD} component (Fig. 1k) for each temperature via symmetrizing the data in Fig. 1g. We find V^{QD} for $I//c$ (Fig. 1k) is much smaller than V^{QD} for $I//a$ (Fig. 1i), while the V^L component due to the electrical contacts' misalignment for both measurements are nearly the same as expected (e.g. see the data at 350K in Fig. 1j). The small V^{QD} component for $I//c$ can be attributed to the small misalignments of the crystallographic axes that occurred during the FIB cutting. The nonreciprocal Hall effect for $I//a$ is also reproduced in all other Hall devices (S2 and HB1) we prepared in this work (see Supplementary Note 3; HB1 stands for a Hall bar device, which will be discussed in detail below). The I - V curves of these two devices (Fig. S5 & S6) show nonreciprocal Hall effect characteristics in the temperature range of 250-360K, but linear behavior below 250K and above 360K.

In addition to DC transport measurements, we have also confirmed the NLHE of NbP through AC transport measurements using the lock-in technique. As shown in Fig. 2b, at room temperature, when an AC was applied along the a -axis, a transverse second-harmonic voltage along the c -axis, $V_{c-aa}^{2\omega}$, was detected and $V_{c-aa}^{2\omega}$ scales quadratically with the input current I^ω . Such second-harmonic voltage is hardly frequency-dependent below 2000 Hz (inset to Fig. 2b), which, together with the linear DC I - V characteristics measured using the two-probe method and the nonlinear Hall voltage's dominance over the longitudinal response exclude the junction effect from the contacts (see Supplementary Note 2 and Figs. S3 and S4). Moreover, when the current was applied to the c -direction, the transverse second-harmonic voltage along the a -axis, $V_{a-cc}^{2\omega}$, was about ten times smaller than $V_{c-aa}^{2\omega}$, consistent with the dependence of the nonreciprocal Hall effect on the current direction discussed above. Besides the second-harmonic Hall voltage response, we also probed the DC rectification voltage V_{c-aa}^{RDC} for $I^\omega//a$ with $V_{c-aa}^{RDC} \propto (I^\omega)^2$ (Fig. 2c), which is also a hallmark of NLHE. The ratio of the rectification voltage to the second-harmonic voltage is about 1.5, close to the theoretical value of $\sqrt{2}$.²⁰ Similar results are also reproduced on device S2 and HB1 (see Supplementary Note 4). Additionally, we also measured the temperature dependence of the NLHE and found $V_{c-aa}^{2\omega}$ and V_{c-aa}^{RDC} exhibit striking peaks near room temperature in all three devices, but becomes zero below 250 K for S1 (200 K for S2 & HB1), as shown in Fig. 2d where $V_{c-aa}^{2\omega}$ and V_{c-aa}^{RDC} are normalized to their peak values. The temperature dependences of $V_{c-aa}^{2\omega}$ and V_{c-aa}^{RDC} agree well with the temperature dependence of the nonreciprocal Hall effect discussed above, indicating that the NLHE is the origin of the nonreciprocal Hall effect. Although the peak temperature of $V_{c-aa}^{2\omega}$ is different among these three samples (356 K for S1, 319 K for S2, and 327K for HB1), their peak profiles are almost the same. Such non-monotonic temperature dependences of the NLHE can be well understood in terms of the theoretically calculated energy dependence of the BCD (see Supplementary Note 2).

The colossal NLHE of NbP is also manifested in its exceptionally large Hall angle θ_H . This is revealed in the DC transport measurements on the bar-like device HB1 with two pairs of voltage

leads (see the inset to Fig. 3d). In those measurements, the DC is applied along the long dimension direction of the device (i.e. the a -axis) and the Hall voltage is measured along the transverse c -axis. The measurements were performed under zero magnetic field. In general, θ_H is defined as $\tan^{-1}(\frac{E_y}{E_x})$, where E_x and E_y represent the longitudinal and transverse (Hall) field respectively. In our experiment configuration, $\theta_H = \tan^{-1}(\frac{E_c}{E_a})$. Since the Hall field probed in our experiment is generated by the NLHE, the Hall field E_c should be proportional to the square of E_a . Hence, $\tan \theta_H \propto E_a$. In other words, $\tan \theta_H$ should be almost linearly dependent on the applied current I_a . This is exactly what we observed in device HB1. The inset of Fig. 3a presents the $\tan \theta_H$ of HB1 as a function of I_a measured at 330K where its NLHE is close to the maximum (Fig. 2d). These data clearly demonstrate the linear dependence of $\tan \theta_H$ on I_a . The value of $\tan \theta_H$ reaches 0.81 at 1 mA, which corresponds to $\theta_H = 39^\circ$. To the best of our knowledge, this angle is larger than any of the previously reported anomalous Hall angles of magnetic conductors^{3,21-28} (Fig. 3a) and can be further increased with a larger current. Nonlinear Hall materials with large Hall angles are recently predicted to be promising candidates for quantum rectification and can find applications in wireless charging and energy harvesting.²⁹

The large Hall angle seen in NbP indicates its NLHE induces a strong Hall field E_c . For instance, at $I_a = 1$ mA, E_c is ~ 228 V/m, reaching 81% of the driving field E_a ($=280$ V/m). We find such a strong Hall field along the transverse (c) direction gives rise to a change of conductivity along the longitudinal (a) direction, an unprecedented transport phenomenon which we term *bulk electric field effect*. This bulk electric field effect is characterized by a second-order conductivity tensor σ_{xyx} , and is closely related to the NLHE originating from Berry curvature dipole. Because the current associated with anomalous velocity is always perpendicular to the applied electric field, the second-order conductivity σ_{ijk} is necessarily antisymmetric in the pair of indices i, j , hence we have

$$\sigma_{caa} = -\sigma_{aca}. \quad (1)$$

This is a remarkable relation relating the nonlinear Hall effect and the bulk electric field effect. Because NbP shows large NLHE due to BCD, we can expect a large bulk electric field effect from Eq.(1).

Figs. 3b & 3c illustrate such a novel exotic quantum transport phenomenon. When the NLHE is not considered (Fig. 3b), the charge transport follows Ohm's law, i.e. $E_a \propto j_a$. However, when the NLHE creates a strong Hall field E_c as shown in Fig. 3c, the longitudinal charge transport is significantly affected by E_c through σ_{aca} , which results in smaller E_a . As a result, the longitudinal conductivity becomes larger compared to the situation without the NLHE, as illustrated by the color contrast between Fig. 3b and 3c. This was verified by our I_a - V_a measurements on HB1, as shown in Fig. 3d which plots the data measured at 330 K. As I_a is increased above 0.4 mA, V_a displays sublinear dependence on I_a , which becomes clear as I_a approaches 1 mA and can be well fitted by including the third-order correction in E_x to j_x (see Supplementary Note 5 for details of the fitting), as shown by the blue fitted curve in Fig. 3d. As I_a is increased to 1 mA, the longitudinal conductivity increases by $\sim 6\%$ based on the data in Fig. 3d.

Because the linear relation between I_a and V_a breaks down, I_a - V_c relation also deviates from the quadratic relation (for more details, see Supplementary Note 5). In the I_a - V_c measurements on HB1, we also observed evidence of the deviation of V_c from being quadratic in I_a . From the I_a - V_c data presented in Fig. 3e, we can see that the deviation of V_c from being quadratic in I_a is clearly discernable as I_a approaches 1 mA, with the deviation magnitude being $\sim 10\%$ at 1 mA, and this data can be fitted by including the fourth-order correction, as shown by the blue fitted curve in Fig. 3e. Such a deviation of V_c from the quadratic dependence on I_a in the large current range was also observed in S1 and S2 (e.g. see Fig. 1h). To further verify the 3rd order correction to E_a and 4th order correction to E_c , we have also performed AC transport measurements on HB1 and observed a 3rd-harmonic longitudinal voltage component $V_a^{3\omega}$ and a 4th-harmonic transverse voltage component $V_c^{4\omega}$ and the magnitudes of $V_a^{3\omega}$ and $V_c^{4\omega}$ are, respectively, approximately agree with the deviation of V_a^ω from the linearity in I_a^ω and the deviation of $V_c^{2\omega}$ from the quadratic dependence in I_a^ω (see Supplementary Note 6 and Fig. S8). It should be noted that, even in the presence of the bulk electric field effect, the transverse field E_c remains quadratic in E_a as long as third- and higher-order current responses are negligible:

$$E_c = -\frac{\sigma_{caa}}{\sigma_{cc}} E_a^2.$$

Our measurements on device HB1 clearly demonstrated this relation. Fig. 3f presents the dependence of E_c on E_a measured at 330 K; E_c show a precise quadratic dependence on E_a even as I_a is increased to ~ 1 mA. Therefore, we conclude that in the range of applied current, the deviation of E_a (E_c) from the linear (quadratic) dependence on j_a comes from the interplay between two *second-order* current responses: the nonlinear Hall effect (σ_{caa}) and the bulk electric field effect (σ_{aca}).

As noted above, strong NLHE may find applications in THz detection and energy harvesting. For a NLHE to be useful, it requires not only working temperature near room temperature but also high responsivity. The NLHE's responsivity R is defined as $E_y^{2\omega}/(E_x^\omega)^2$ (or $E_y^{DC}/(E_x^{DC})^2$, where $E_y^{2\omega}$ (E_y^{DC}) and E_x^ω (E_x^{DC}) are the output and input electric fields, respectively. The NLHE of NbP exhibits very large responsivity, with the maximal R value reaching $\sim 1.9 \times 10^{-3} \text{ mV}^{-1}$ at 330 K for HB1, which is comparable to that of BaMnSb₂²⁰, but several orders of magnitude larger than those of previously reported intrinsic NLHE in other material systems (see Supplementary Note 7 and Fig. S9). It is worth pointing out that since our devices were fabricated via FIB machining, the surface damage by the ion beam should be considered. In the longitudinal resistivity measurements of device HB1, we indeed observed signs of surface damage (see Supplementary Notes 8&9 for more discussions). The R value of the NbP's NLHE might be further increased if the surface damage caused by the ion beam could be avoided. The large NLHE's responsivity of NbP near room temperature makes NbP a promising candidate material for developing high-sensitivity quantum sensor to detect THz radiation, which could have high potential to impact a wide variety of applications such as future 6G communication technology and THz imaging for security and medical applications. In our work, we have demonstrated NbP's Hall device can be used as a sensor to perform wireless microwave detection. As shown in Fig. 4a, a signal generator was used to generate a 2.4GHz radio frequency (RF) signal which was transmitted to the device S1 through a pair of antennas. When the antenna was connected to the terminals along the a -axis of the device,

the signal analyzer connected to the terminals along the *c*-axis probed a strong second-harmonic signal. The power of the detected signal is quadratic to the source power (Fig. 4b), consistent with the NLHE demonstrated above.

Methods

Crystal Growth

The single crystals of NbP were synthesized using a chemical vapor transport (CVT) method via the following procedures.³⁰ Firstly, the stoichiometric mixture of Ta and P powder was sealed in an evacuated quartz tube and sintered at 800°C for 48 hours. Secondly, we ground the sintered NbP polycrystalline material into powder inside a glovebox and then sealed it into another evacuated quartz tube with iodine as a transport agent (13.5 mg cm⁻³). Then the quartz tube was placed into a double-zone furnace with the temperature set at 850°C for the cold zone (source) and 950°C for the hot zone (sink). After one week of the CVT growth, large shiny NbP single crystals with flat (0 0 1) surfaces can be found near the hot end. We confirmed the grown NbP crystals have the desired structure and composition from X-ray diffraction and Energy-dispersive X-ray spectroscopy analyses.

Micrometer Hall Device Fabrication

Microscale devices in the cross and Hall bar geometry were fabricated by focused ion beam (FIB) cutting using FEI Helios NanoLab 660 and FEI Scios 2 dual beam SEM. First, we cut NbP thin lamellar samples with typical dimensions of 15 × 15 × 3 μm (cross devices) or 20 × 10 × 2 μm (Hall bar device) from millimeter-scale crystals using FIB and then lift and transferred it to Si substrates. The FIB cutting was made along the *a*-axis on the (0 0 1) surface so that the edges of the lamellar sample are approximately parallel to the crystallographic *a*- and *c*-axis respectively (see the inset to Fig. 1e). Second, we further cut the lamellar crystal into a cross-shape or bar-shape with FIB and deposited Pt wires and pads for electrical contacts (see Supplementary Note 1 for detailed procedures).

Electrical Transport Measurements

The electrical transport measurements were conducted inside a Quantum Design Physical Property Measurement System (PPMS). The AC and DC driving currents were, respectively, generated by a Keithley 6221 and a Keithley 6220 precision current sources. The AC and DC voltages were measured by a Stanford Research SR860 lock-in amplifier and a Keithley 2182A nanovoltmeter, respectively.

Radio Frequency Measurement

A Keysight MXG Vector signal generator was used to generate RF signals. A pair of TP-link antennas were used to transmit and receive wireless signals. The receiving antenna is connected to one arm of the cross-like device made of NbP while the opposite arm was grounded. The signals from the two terminals in the other direction were measured by an Agilent CXA signal Analyzer.

Data availability

The authors declare that all the data that support the findings of this study are available within the paper and Supplementary Information. Additional relevant data are available from the corresponding authors upon reasonable request. Source data are provided with this paper.

Reference

- 1 Zhang, Y. & Fu, L. Terahertz detection based on nonlinear Hall effect without magnetic field. *Proceedings of the National Academy of Sciences* **118**, e2100736118, doi:10.1073/pnas.2100736118 (2021).
- 2 Tokura, Y. & Nagaosa, N. Nonreciprocal responses from non-centrosymmetric quantum materials. *Nature Communications* **9**, 3740, doi:10.1038/s41467-018-05759-4 (2018).
- 3 Li, P. *et al.* Giant room temperature anomalous Hall effect and tunable topology in a ferromagnetic topological semimetal Co₂MnAl. *Nature Communications* **11**, 3476, doi:10.1038/s41467-020-17174-9 (2020).
- 4 Rikken, G. L. J. A. & Wyder, P. Magnetoelectric Anisotropy in Diffusive Transport. *Physical Review Letters* **94**, 016601, doi:10.1103/PhysRevLett.94.016601 (2005).
- 5 Wakatsuki, R. *et al.* Nonreciprocal charge transport in noncentrosymmetric superconductors. *Science Advances* **3**, e1602390, doi:10.1126/sciadv.1602390 (2017).
- 6 Yasuda, K. *et al.* Nonreciprocal charge transport at topological insulator/superconductor interface. *Nature Communications* **10**, 2734, doi:10.1038/s41467-019-10658-3 (2019).
- 7 Yasuda, K. *et al.* Large non-reciprocal charge transport mediated by quantum anomalous Hall edge states. *Nature Nanotechnology* **15**, 831-835, doi:10.1038/s41565-020-0733-2 (2020).
- 8 Itahashi, Y. M. *et al.* Nonreciprocal transport in gate-induced polar superconductor SrTiO₃. *Science Advances* **6**, eaay9120, doi:10.1126/sciadv.aay9120 (2020).
- 9 Li, Y. *et al.* Nonreciprocal charge transport up to room temperature in bulk Rashba semiconductor α -GeTe. *Nature Communications* **12**, 540, doi:10.1038/s41467-020-20840-7 (2021).
- 10 Zhang, Z. *et al.* Controlled large non-reciprocal charge transport in an intrinsic magnetic topological insulator MnBi₂Te₄. *Nature Communications* **13**, 6191, doi:10.1038/s41467-022-33705-y (2022).
- 11 Sodemann, I. & Fu, L. Quantum Nonlinear Hall Effect Induced by Berry Curvature Dipole in Time-Reversal Invariant Materials. *Physical Review Letters* **115**, 216806, doi:10.1103/PhysRevLett.115.216806 (2015).
- 12 Ma, Q. *et al.* Observation of the nonlinear Hall effect under time-reversal-symmetric conditions. *Nature* **565**, 337-342, doi:10.1038/s41586-018-0807-6 (2019).
- 13 Kang, K., Li, T., Sohn, E., Shan, J. & Mak, K. F. Nonlinear anomalous Hall effect in few-layer WTe₂. *Nature Materials* **18**, 324-328, doi:10.1038/s41563-019-0294-7 (2019).
- 14 Kumar, D. *et al.* Room-temperature nonlinear Hall effect and wireless radiofrequency rectification in Weyl semimetal TaIrTe₄. *Nature Nanotechnology* **16**, 421-425, doi:10.1038/s41565-020-00839-3 (2021).
- 15 Dzsaber, S. *et al.* Giant spontaneous Hall effect in a nonmagnetic Weyl-Kondo semimetal. *Proceedings of the National Academy of Sciences* **118**, e2013386118, doi:10.1073/pnas.2013386118 (2021).
- 16 Qin, M.-S. *et al.* Strain Tunable Berry Curvature Dipole, Orbital Magnetization and Nonlinear Hall Effect in WSe₂ Monolayer. *Chinese Physics Letters* **38**, 017301, doi:10.1088/0256-307x/38/1/017301 (2021).
- 17 Huang, M. *et al.* Giant nonlinear Hall effect in twisted bilayer WSe₂. *National Science Review*, nwac232, doi:10.1093/nsr/nwac232 (2022).

- 18 Tiwari, A. *et al.* Giant c-axis nonlinear anomalous Hall effect in Td-MoTe₂ and WTe₂. *Nature Communications* **12**, 2049, doi:10.1038/s41467-021-22343-5 (2021).
- 19 He, P. *et al.* Quantum frequency doubling in the topological insulator Bi₂Se₃. *Nature Communications* **12**, 698, doi:10.1038/s41467-021-20983-1 (2021).
- 20 Min, L. *et al.* Strong Room-Temperature Bulk Nonlinear Hall Effect in a Spin-Valley Locked Dirac Material. *arXiv*, doi:10.48550/arXiv.2212.06230 (2022).
- 21 Suzuki, T. *et al.* Large anomalous Hall effect in a half-Heusler antiferromagnet. *Nature Physics* **12**, 1119-1123, doi:10.1038/nphys3831 (2016).
- 22 Singha, R., Roy, S., Pariari, A., Satpati, B. & Mandal, P. Magnetotransport properties and giant anomalous Hall angle in the half-Heusler compound TbPtBi. *Physical Review B* **99**, 035110, doi:10.1103/PhysRevB.99.035110 (2019).
- 23 Zhu, Y. *et al.* Exceptionally large anomalous Hall effect due to anticrossing of spin-split bands in the antiferromagnetic half-Heusler compound TbPtBi. *Physical Review B* **101**, 161105, doi:10.1103/PhysRevB.101.161105 (2020).
- 24 Wu, F. *et al.* Electrical transport properties of perpendicular magnetized Mn-Ga epitaxial films. *Applied Physics Letters* **96**, 042505, doi:10.1063/1.3298363 (2010).
- 25 Sakai, A. *et al.* Giant anomalous Nernst effect and quantum-critical scaling in a ferromagnetic semimetal. *Nature Physics* **14**, 1119-1124, doi:10.1038/s41567-018-0225-6 (2018).
- 26 Kim, K. *et al.* Large anomalous Hall current induced by topological nodal lines in a ferromagnetic van der Waals semimetal. *Nature Materials* **17**, 794-799, doi:10.1038/s41563-018-0132-3 (2018).
- 27 Liu, E. *et al.* Giant anomalous Hall effect in a ferromagnetic kagome-lattice semimetal. *Nature Physics* **14**, 1125-1131, doi:10.1038/s41567-018-0234-5 (2018).
- 28 Shen, J. *et al.* 33% Giant Anomalous Hall Current Driven by Both Intrinsic and Extrinsic Contributions in Magnetic Weyl Semimetal Co₃Sn₂S₂. *Advanced Functional Materials* **30**, 2000830, doi:10.1002/adfm.202000830 (2020).
- 29 Onishi, Y. & Fu, L. High-efficiency quantum rectification via nonlinear Hall effect. *arXiv*, doi:10.48550/arXiv.2211.17219 (2022).
- 30 Shekhar, C. *et al.* Extremely large magnetoresistance and ultrahigh mobility in the topological Weyl semimetal candidate NbP. *Nature Physics* **11**, 645-649, doi:10.1038/nphys3372 (2015).

Acknowledgments

This work is primarily supported by the US National Science Foundation under grant DMR 2211327. L.Min, L.Mia, N.A., and Z.M. also acknowledge the partial support from NSF through the Materials Research Science and Engineering Center DMR 2011839 (2020 - 2026). The work at Massachusetts Institute of Technology was supported by the U.S. Army Research Laboratory and the U.S. Army Research Office through the Institute for Soldier Nanotechnologies, under Collaborative Agreement Number W911NF-18-2-0048. LF was partly supported by the David and Lucile Packard Foundation. Y.O. thanks the support from Funai Overseas Scholarship.

Author contributions

The crystal growth and transport measurements were carried out and analyzed by L.Min & Z.M. The device fabrications were performed by L.Min, L.Mia, N.A., and Z.M. The theoretical work was done by Y.Z., Y.O., and L.F. Z.X. performed the wireless microwave detection experiment. The paper was written by L.Min, Y.O., L.F., and Z.M. with inputs from other authors. Z.M. supervised the experimental part of this work and L.F. supervised the theoretical part.

Competing interest declaration.

The authors declare no competing interests.

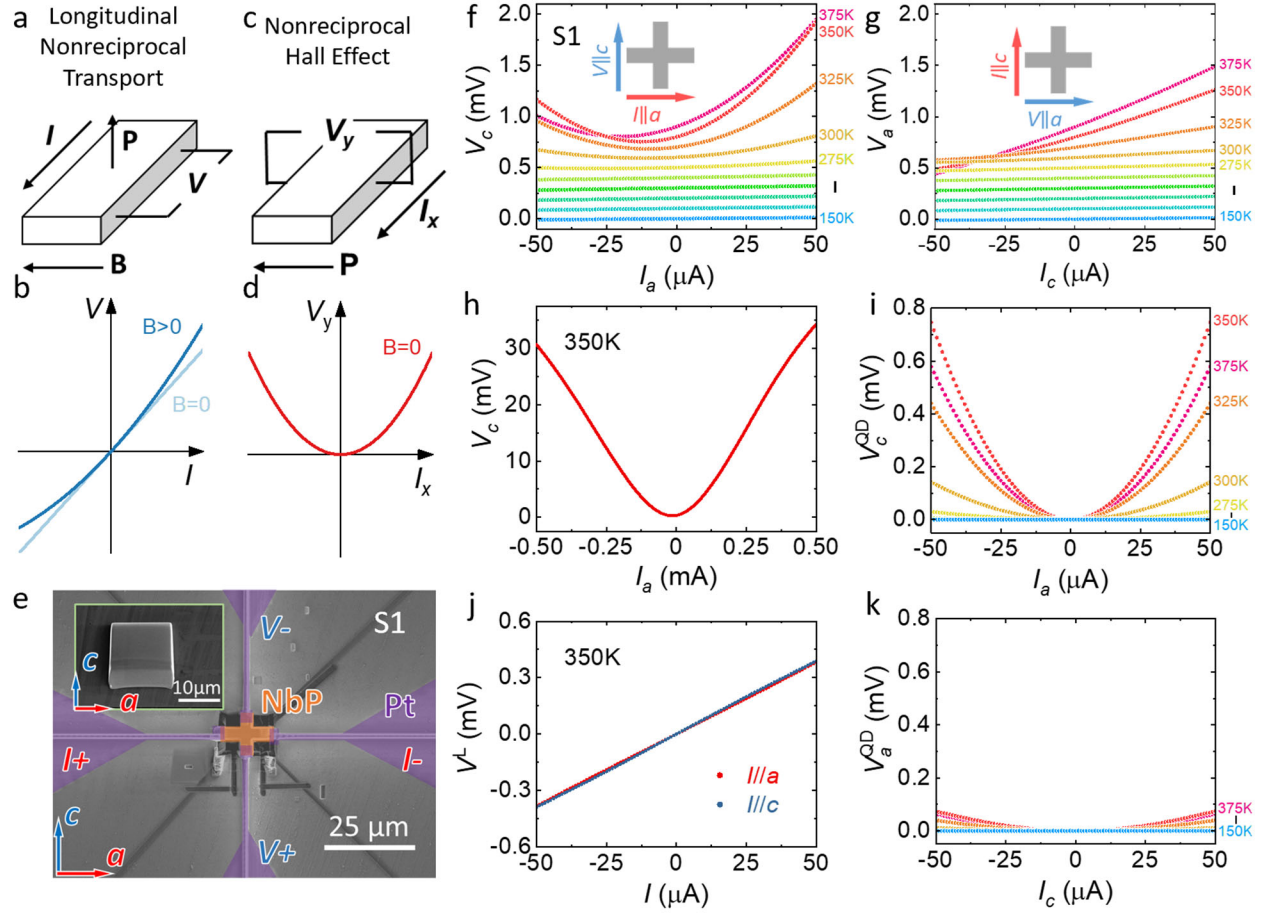


Fig.1 Nonreciprocal Hall effect in NbP. (a & c) Schematic of the longitudinal nonreciprocal (NR) transport (a) and the nonreciprocal Hall effect (b) in a polar system with a polar axis along the z-axis. (b & d) Schematic DC I - V curves of the Ohmic transport (light blue in b), the longitudinal nonreciprocal transport (dark blue in b), and the nonreciprocal Hall effect (d). (e) SEM image of a cross-shape Hall device of NbP (labeled with S1). Inset: the image of the lamellar NbP crystal used for fabricating device S1. The edges of this lamellar crystal are approximately parallel to the a - and c -axis respectively. (f & g) DC I - V characteristics measured with the current applied along the a -axis (f) and the c -axis (g) respectively at various temperatures for S1. The I - V curves for $I//a$ exhibit distinct parabolic-like behavior from 300K to 375K, while in the same temperature range, the I - V curves for $I//c$ are quasi-linear. (h) DC I - V curve measured to ± 0.5 mA at 350K. (i, k) The nonreciprocal Hall voltage $V^{QD}(\propto I^2)$ component due to the NLHE for $I//a$ (i) and $I//c$ (k). (j) The longitudinal voltage $V^L(\propto I)$ component due to the electric contacts' misalignment (j & k) at 350K for $I//a$ and $I//c$. V^{QD} and V^L are extracted respectively via symmetrizing and anti-symmetrizing the data in panels (f) and (g).

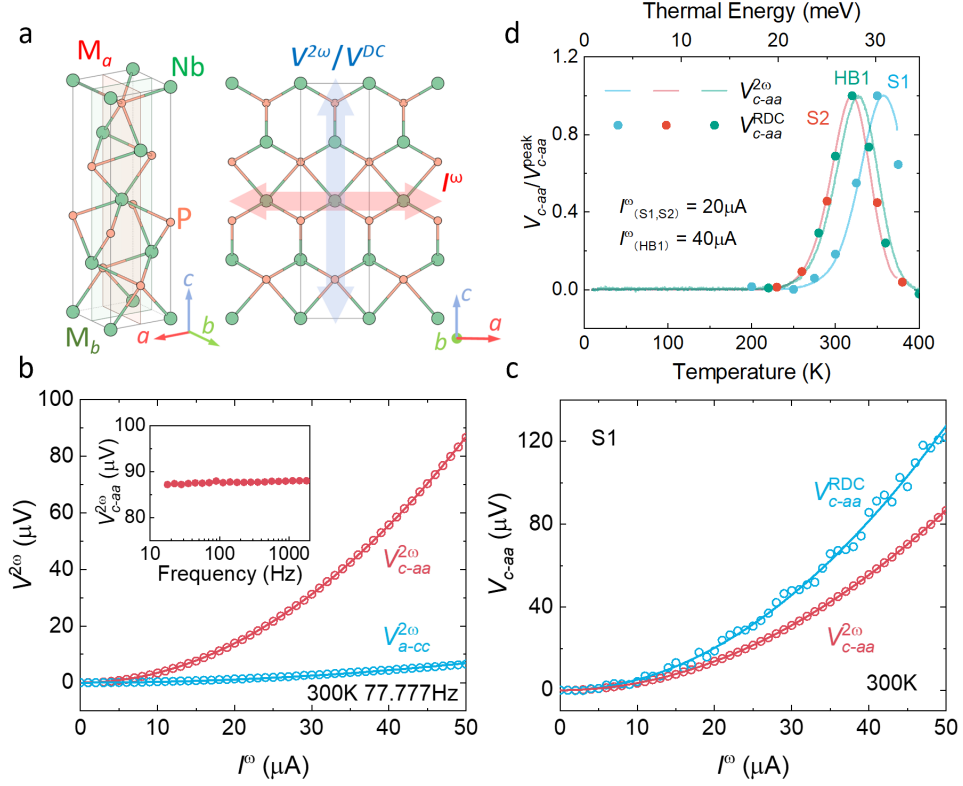


Fig. 2. Colossal intrinsic NLHE in NbP near room temperature. (a) Left: Crystal structure of NbP. M_a and M_b represent two vertical mirror planes perpendicular to the a and b crystallographic axis respectively. Right: illustration of NLHE of NbP, i.e. an alternating current applied along the a -axis drives a second-harmonic and a rectified DC Hall voltage along the c -axis. (b) The second-harmonic Hall voltage $V_{c-aa}^{2\omega}$ of device S1 vs. the input current I^ω for the current applied to the a - (red) and c -axis (blue), respectively, at 300K. Inset: the frequency dependence of the second-harmonic Hall voltage under the input current of 50 μA applied along the a -axis at 300K. (c) The second-harmonic Hall voltage $V_{c-aa}^{2\omega}$ and rectified Hall voltage V_{c-aa}^{RDC} vs. the input current I^ω at 300K for S1. (d) Normalized second-harmonic and rectified Hall voltages ($V_{c-aa}^{2\omega}$, V_{c-aa}^{RDC}) as a function of temperature for S1, S2, and HB1 measured with an input current applied along the a -axis. $V_{c-aa}^{2\omega}$ and V_{c-aa}^{RDC} are presented with lines and filled circles respectively.

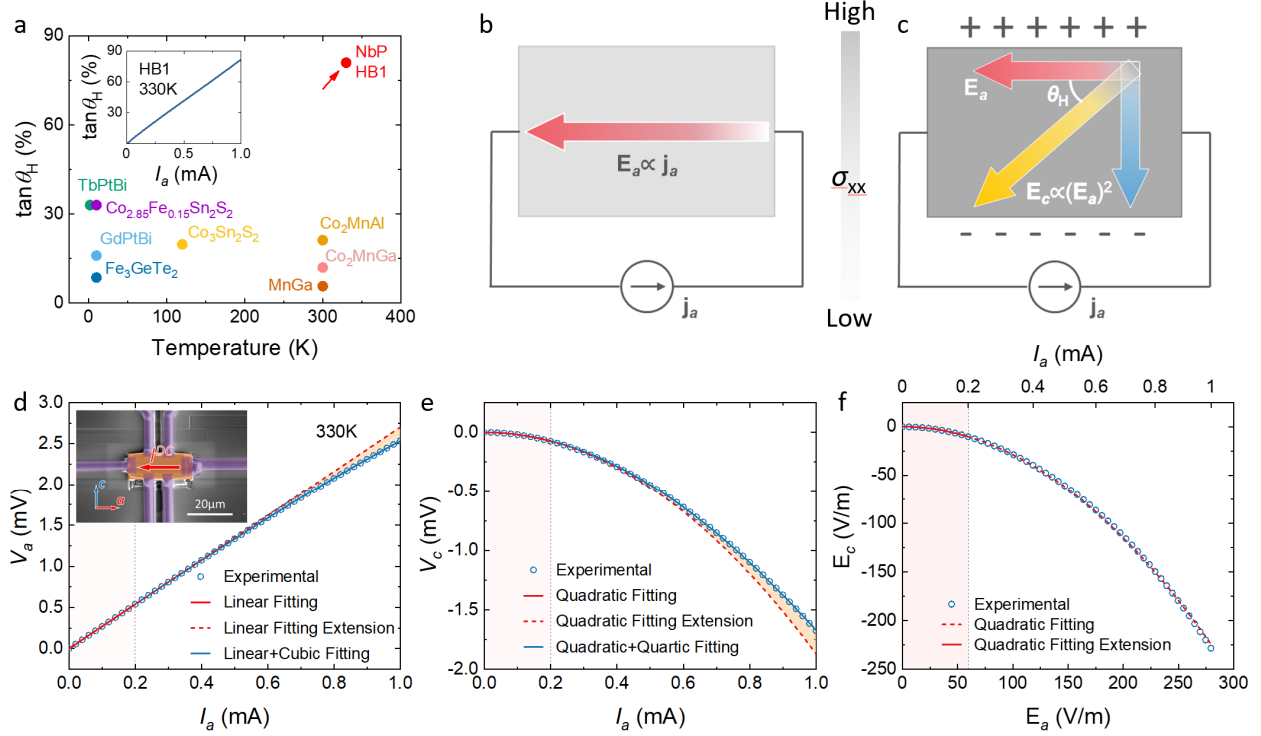


Fig. 3. Bulk electric field effect induced by the NLHE in NbP. (a) The comparison of the Hall angle $\tan \theta_H$ between NbP and other conductors showing large anomalous Hall effect. Inset: the Hall angle $\tan \theta_H$ of HB1 versus the DC input current I_a . Schematic of electric field distribution in conductors with (b) or without (c) the NLHE under zero magnetic field. The color contrast between (b) and (c) represents the variation of longitudinal σ_{xx} . The large Hall field E_y in (c) increases σ_{xx} compared to the situation without the NLHE. (d) The longitudinal voltage V_x versus the DC input current I_a measured on the Hall bar device HB1. Inset: the SEM Image of device HB1. (e) The transverse voltage V_c versus the DC input current I_a measured on HB1. The first 11 experimental data points in the low current range marked in pink were used to conduct the linear (d) or quadratic (e) fitting (red solid lines), and then the fitted curves were extended to the whole current range (red dashed lines). From the area marked in orange, we can see that V_a clearly deviates from linear dependence and V_c deviates from the quadratic dependence on I_a as I_a approaches 1 mA. The blue solid lines represent the fits to the theory which considers 3rd-order correction to E_x and 4th-order correction to E_y caused by the NLHE and electric field effect (see text). (f) The transverse electric field E_c versus the longitudinal electric field E_a . The quadratic fitting and extension method is the same as that used in panels (d) and (e). $E_c - E_a$ maintains a quadratic dependence even when the $V_a - I_a$ ($V_c - I_a$) characteristics deviates from linear (quadratic) dependence, consistent with the theoretical prediction. All the data presented here were measured at 330K where device HB1 shows a maximal nonlinear Hall voltage.

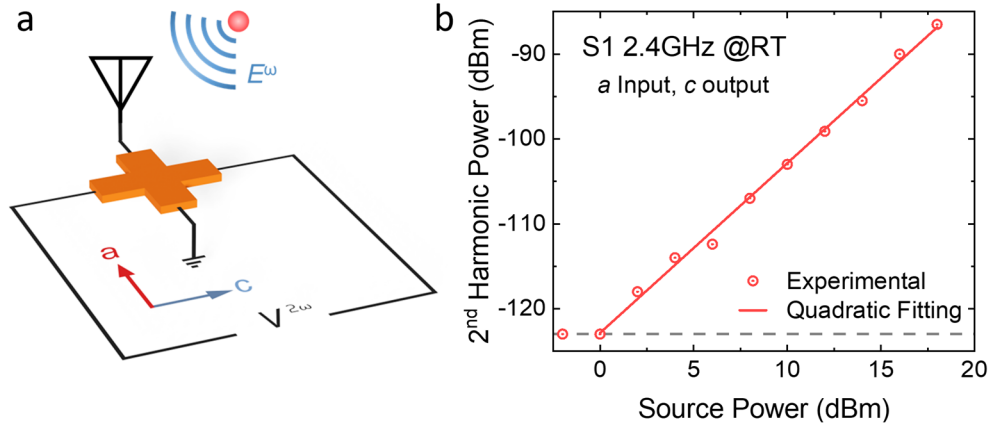


Fig. 4. Room temperature wireless microwave detection based on the NLHE of NbP. (a) Schematic of the experiment setup for wireless microwave detection. A pair of antennas are used to transmit and receive wireless signals. (b) Measured second-harmonic output power versus input source power when the antenna is connected along the a -axis. The solid line represents the fit of the quadratic relationship between the output power and the input power.